Direct measurement of the electron density in electron-beam-irradiated Ar-F_2 gas mixtures by time-resolved interferometry

Z. Rozenberg, M. Lando, and M. Rokni
Racah Institute of Physics, Hebrew University of Jerusalem, Jerusalem, Israel
(Received 14 August 1986)

The secondary-electron density in electron-beam-irradiated Ar-F_2 gas mixtures has been measured for the first time using time-resolved interferometry at 9.6 μm. Measurements were performed for gas mixtures with various F_2 concentrations between 0.0025% and 2% and total pressures between 0.5 and 2 atm. The e-beam pulse was 350 nsec long at an energy of 150 keV and current density ranging between 0.025 and 6.3 A/cm^2. From the dependence of the measured steady-state electron density on fluorine concentration, the rate constant for electron attachment to fluorine at zero electric field has been determined for the first time. For a given e-beam current density, the attachment rate constant is found to be a decreasing function of the fluorine concentration, while for a given F_2 concentration it is found to be an increasing function of the e-beam current density. The results are interpreted as a manifestation of the variation of the electron energy distribution as a function of F_2 concentration and e-beam current density. The predictions of a theoretical kinetic model for calculation of the electron distribution function, taking into account the removal of slow electrons by attachment, are compared with the experimental results. It is concluded that for the range of the experimental parameters presented above, the net effect of adding fluorine to the gas mixture is an increase in the average electron energy, caused by removal of low-energy electrons by attachment.

I. INTRODUCTION

Since their discovery, the rare-gas—fluoride lasers have been intensively investigated as high-power and efficient uv lasers. Until now most of the experimental work has been focused on the heavy-particle kinetics, their role in the formation and quenching of the lasing species, and their effect on laser extraction.[1]

The secondary electrons have an equally important role in the kinetics of these lasers. They serve as main agents in the formation of excited species.[1] These include excited species that contribute to the gain in the laser medium, as well as those which contribute to absorption losses. Secondary electrons also can quench excited species and in many cases the quenching of the upper laser level by electrons is very important.[2–4] Another important role of the secondary electrons is the mixing of the excited species such as the B and C states of the lasing exciplex, by energy transfer.

Until now the information on the secondary electrons in these lasers has been obtained by indirect methods. In general electron densities have been calculated by complex kinetic codes using available rate constants and their energy distribution has been calculated by Boltzmann codes using available electron-impact cross sections.[5–10] The experimental information on the secondary electrons has been indirect in the sense that the quantities compared with experimental results have been code-calculated rate constants, for processes such as electron attachment and heavy-particle excitation by electron impact.

In this paper we present the results of the first direct measurement of the electron density in electron-beam-irradiated ArF_2 gas mixtures. The measurements were performed by time-resolved infrared interferometry at 9.6 μm using a Mach-Zehnder interferometer. This type of measurement is direct in the sense that the measured refractive index increment due to the free electrons is dependent only on the electron density.[11] From the dependence of the measured electron density on the fluorine density, the electron-attachment rate constant in an e-beam-pumped system (without an external electric field) has been obtained experimentally for the first time and its dependence on the fluorine concentration and electron-beam current density has been studied. All previous measurements of the attachement rate constant were performed by applying an external electric field to the plasma and measuring either the resulting steady-state current[12,13] or its decay time after the termination of the e-beam pulse,[14,15] as the function of the density of the attaching molecule. The current decay measurements assume that the drift velocity is constant during the measurement time. This assumption is questionable because the decay of the electron density and the excited-state density after the termination of the e-beam pulse could result in an appreciable change in the electron energy distribution which in turn would cause a change in the drift velocity. On the other hand, the steady-state current measurements necessitate the knowledge of the drift velocity for the proper gas mixtures used and this information is not available in most cases. Clearly, neither of these methods could provide attachment rate constants at zero external field. Deriving the attachment rate constant from direct measurement of the electron density, as described in Secs. II—V, is free from these limitations and disadvantages.

II. EXPERIMENTAL PROCEDURE

The experimental setup is described schematically in Fig. 1. The experimental cell was located within one leg of a Mach-Zehnder interferometer, which was aligned to work at the zeroth order (full phase-front interference). An Apollo CO_2 laser working at 9.6 μm was used as the radiation source. The probe beam was aligned along the 23-cm-long active medium and perpendicular to the e beam. The optical signal was detected by a HgCdTe infrared detector with a rise time of 10 nsec and an active area of 3×10^{-4} cm^2. The output signal of the infrared detector was stored and analyzed using a 6500 Biomation digitizer with a resolution of 2 nsec per channel, interfaced with an Apple computer. The electron beam was provided by a cold cathode cable gun which produced 350-nsec-long pulses of 150-keV electrons at current densities up to 12 A/cm^2. The rise and fall times of the e-beam pulse were less than 10 nsec. The beam entered the experimental cell through a window of Kapton foil 50 μm thick, 23-cm wide and 1-cm high. The distance between the foil and the probe beam was 5 mm. By placing mesh attenuators between the e-beam anode and the foil, the current density could be reduced down to 10^{-2} A/cm^2.

99.999% pure argon and 98% pure fluoride, obtained from Matheson gas products, were used. The gases were premixed in a separate mixing manifold and then transferred to the experimental manifold in stainless-steel tanks. All portions of the gas handling system including the experimental cell and the stainless-steel tanks were passivated with fluorine for a few hours before use. The quality of the passivation and the reduction of fluorine density were checked by monitoring the fluorine absorption at 2537 Å. It was found that the fluorine concentration in the tanks was constant for more than three months while in the experimental cell it was reduced by 10% after 30 minutes. Therefore, during the measurements the gas mixture was held in the experimental cell no longer than 10 minutes. All portions of the gas handling system were pumped down to 10^{-5} torr before each refill.

9.6 μm rather than visible interferometry was used to ensure that the measured time-dependent refractive index increment was due to the free electrons and with negligible contribution from excited species. For frequencies considerably higher than the plasma frequency the contribution of the free electrons to the refractive index at frequency ω is given by[11]

$$\Delta n(\omega)\approx -\frac{\omega_p^2}{2\omega^2}\ , \tag{1}$$

where ω_p is the plasma frequency given in MKS units by

$$\omega_p^2=\frac{n_e e^2}{m_e\epsilon_0}\ , \tag{2}$$

where n_e is the density of the free electrons, e and m_e are the electron charge and mass, respectively, and ϵ_0 is the vacuum permeability. From Eq. (1) it is clear that the contribution of the free electrons to the refractive index increases quadratically with the wavelength. To evaluate the contribution of the excited states, the specific refractive index[16] for a variety of excited states of argon was numerically calculated. This was done using the oscillator strengths and spectroscopic data for more than 300 transitions given by Weise *et al.*[17] The results showed that at a visible wavelength the contribution of an excited atom in one of the four lowest excited states of argon ($1S_5$, $1S_4$, $1S_3$, and $1S_2$ in Paschen notation) was comparable to that of a free electron. On the other hand, the same calculation showed that at 9.6 μm the contribution of the different excited states of argon was negligible compared to that of the free electrons. Unfortunately a similar calculation for transitions among the different excited states of molecular species such as Ar_2^*, ArF^*, and Ar_2F^* could not be done because of lack of necessary spectroscopic data. However, the contribution of the electronic transitions of the excited molecular species is expected to be small compared to that of the atomic excited states because of the vibrational-rotational splitting of each electronic level. On the other hand, the contribution of the vibrational-rotational transitions is negligible because of their relatively small Einstein coefficients. To further substantiate this conclusion, the absorption of the active medium at 9.6 μm was measured. It was found that no detectable absorption at 9.6 μm was monitored for any of the experiments reported here.

The response of the interferometer output to a phase shift is of a sinusoidal form:[18]

$$I=I_1+I_2+2(I_1I_2)^{1/2}\cos\left[\frac{2\pi L}{\lambda}\Delta n+\phi\right]\ , \tag{3}$$

where Δn is the refractive index increment, L is the length of the active medium, and ϕ is the phase shift caused by the initial difference of optical path length between the two interferometer branches. I_1 and I_2 are the intensities of the probe beam and the reference beam, respectively. The equilibrium working point of the interferometer, i.e., the point where the refractive index measurement starts, was chosen at the center of the linear portion of the sinusoidal response function, i.e., for $\phi=(2j+1)\pi/2$ where j is an integer. This was done by the following method: One of the interferometer mirrors was mounted on a piezoelectric crystal (see Fig. 1), which was driven by an 800-V, 50-Hz ac power supply. Thus the interferometer was forced to pass through the working point 200 times per second. The 800-V drive was sufficient to cause

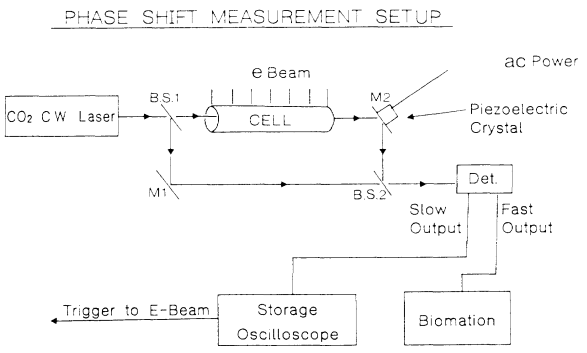

FIG. 1. Schematic description of the experimental setup.

a phase shift of at least 2π in each cycle. The e beam was triggered when the interferometer passed through the working point. Since the time scale of the measured pulse of electron density was short by at least 3 orders of magnitude compared to both the period of the piezoelectric drive and the characteristic time scale of acoustic and mechanical disturbances, we could assume that the interferometric system stood still at the proper working point during the measurement period. Moreover, this large difference in the characteristic time scales enables us to split the output signal of the infrared detector into a fast output (above 100 kHz) and a slow output, using electronic filters. The fast output carried the measured signal and was connected to the Biomation. The slow output was connected to a Tektronix 549 oscilloscope, which monitored the response of the interferometer to the sinusoidal motion of the mirror which was attached to the piezoelectric crystal. The triggering signal for the e beam was supplied by this oscilloscope whenever the interferometer passed through the appropriate working point. The jitter in the triggering by this method was less the 10 nsec.

III. RESULTS

Figure 2(a) shows a typical signal of the fast output of the ir detector, illustrating the variation of the intensity at the interferometer output, as a function of time, as described by Eq. (3). Figure 2(b) shows the corresponding pulse of the electron density which was derived from the data of Fig. 2(a), using Eqs. (1)—(3). As described in Sec. II, the e beam is fired at the proper working point where the initial contribution of the third term in Eq. (3) is zero. With the onset of the e-beam pulse, the intensity first decreases with increasing electron density, reaching a minimum at the point where the phase shift is $\pi/2$. Then the intensity increases again reaching a flat portion, corresponding to a quasi-steady-state electron density. After the termination of the e-beam pulse, the electron density decreases; the signal again passes through a minimum when the phase shift reaches again the value of $\pi/2$ and then decays back to the working point value when the electron density reaches zero.

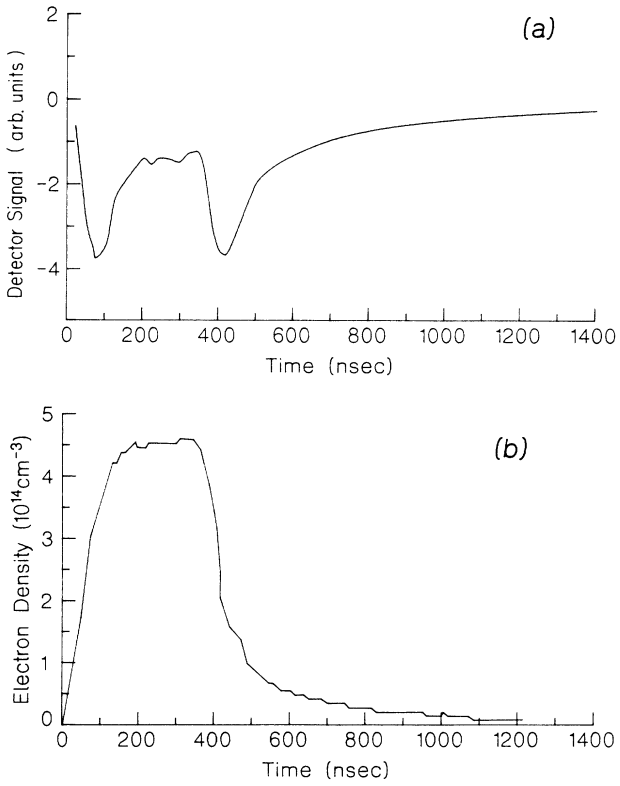

FIG. 2. (a) Typical signal of the interferometric measurement. (b) The corresponding decoded signal, i.e., electron density vs time.

To derive the phase-shift pulse from the measured output signal using Eq. (3), it is necessary to know the peak-to-peak value of the modulated signal $[4(I_1I_2)^{1/2}]$. For phase shifts larger than $\frac{3}{2}\pi$ (corresponding to electron densities larger than 7.5×10^{14} cm^{-3} in our case), this information was provided by the minima and maxima of the measured signal. But for our experimental conditions such high electron densities could be obtained only with pure argon and at high e-beam currents. For phase shifts smaller than $\frac{3}{2}\pi$, this information was obtained by using the peak-to-peak value of the slow output signal multiplied by an appropriate calibration factor which in our case was 0.06. This was done after ensuring that the ratio of the peak-to-peak signal of the fast output to that of the slow output was constant and independent of the CO_2 laser intensity and of the interferometer geometry, as expected. From the measured phase shift the electron density was calculated using Eqs. (1)—(3). It should be emphasized that the sign of the measured phase-shift increment due to the plasma was checked by comparison to the phase shift caused by unidirectional motion of the interferometer mirror and found to be negative, as expected for free electrons.

Figure 3 shows the measured steady-state electron density as a function of fluorine concentration and e-beam current density. Each point in Fig. 3 is the average result of measurements performed at gas mixture pressures

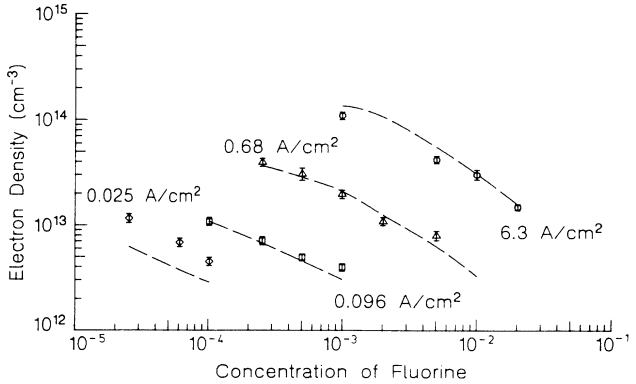

FIG. 3. Comparison of measured electron density as a function of fluorine concentration and electron-beam current density with code predictions (dashed lines).

ranging between 0.5 and 2 atm. Within the limits of the error bars, the measured electron density for a given e-beam current density was independent of the total pressure and depended only on the fluorine concentration. This behavior is expected when the electron-loss mechanism is attachment dominated since both the production rate and the loss rate of the secondary electrons increase linearly with total pressure. The rate equation for the secondary electron density can be written as

$$\frac{dn_e}{dt} = R - \beta[F_2]n_e - \alpha n_e[Ar_2^+] , \quad (4)$$

where R is the production rate of the secondary electrons in the gas by the e-beam, β is the fluorine attachment rate constant, α is the rate constant for recombination of electrons with argon molecular ions, and $[F_2]$ and $[Ar_2^+]$ are the densities of fluorine and the molecular ions, respectively. β for fluorine is of the order of 10^{-9} $cm^3 sec^{-1}$,[12–15] while α is of the order of 10^{-7} $cm^3 sec^{-1}$ (Ref. 19) for electrons with average energy of abut 1 eV. In Eq. (4) electron recombination with atomic ions and diffusion of electrons to the walls have been neglected because, under our experimental conditions, both processes are very slow compared to electron loss by attachment. As will be shown in Sec. IV, for all the experimental points of Fig. 3, the electron-loss rate by recombination is less than 10% of the loss rate by attachment. Thus we conclude that the secondary electron loss is attachment dominated for all experimental points shown in Fig. 3.

From Eq. (4) one can expect the steady-state electron density under attachment dominated conditions to be inversely proportional to the fluorine concentration. However, from Fig. 3 it is obvious that this is not the case. This is because, as will be shown subsequently, β is indirectly dependent on the fluorine concentration through the dependence of the electron density distribution on the fluorine concentration.

To obtain the electron-attachment rate to fluorine using the measured steady-state electron densities and neglecting the recombination term in Eq. (4), it is necessary to know the rate of the secondary-electron production by the e beam, R. The attachment rate cannot be derived from the decay of the electron density after the termination of the e-beam pulse because of the following reason. After the end of the e-beam pulse the secondary electrons cool down, resulting in an increasing attachment rate with time. Thus, after the termination of the e-beam pulse the electron density decays faster than exponential. This is seen in Fig. 4 which shows a semi-log plot of a typical decay of the electron density for ArF_2 mixtures.

The rate of production of the secondary electrons R was derived for the various e-beam current densities and gas pressures used by the following procedure. Since for a given gas pressure, R is directly proportional to the e-beam current density,[20] it is sufficient to determine its value at one current density. Also, e-beam deposition code calculations by Tekula[21] show that for 150-keV electrons and argon the energy deposition by the e beam at 5 mm from the foil increases linearly with pressure within 5%, between pressures of 0.5 and 2 atm as in our case. Therefore, it is sufficient to determine experimentally the

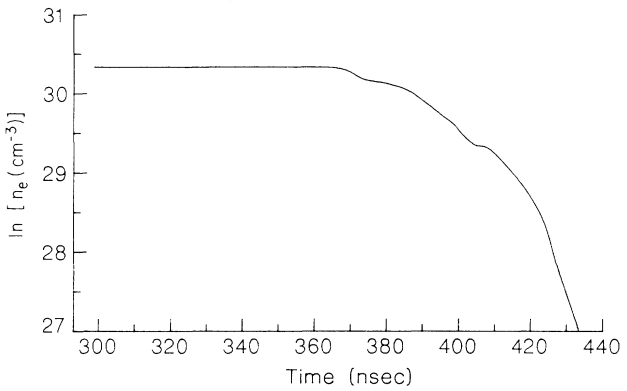

FIG. 4. Semi-log plot of a typical decay of the electron density after the termination of the e-beam pulse.

value of R for a given current density and a given pressure. To do that, the electron density was measured for pure argon at a pressure of 1 atm and at an e-beam current density of 25 mA/cm^2. At such a low current density, the density of the molecular ions during the 350-nsec-long e-beam pulse is so low that the loss of electrons by recombination is negligible compared to their production rate. Such a condition is manifested experimentally by a linear increase of the measured secondary electron density during the e-beam pulse. The value of R for this case was determined by measuring the slope of the electron density as a function of time and was found to be 2.7×10^{19} $cm^3 sec^{-1}$.

Using the derived values for R and the measured steady-state electron densities of Fig. 3, the attachment-rate constant β could be determined using the relation

$$\beta = \frac{R}{n_e[F_2]} . \quad (5)$$

Figure 5 shows the derived attachment rate constant as a function of fluorine concentration and e-beam current density. We note that for a given e-beam current density, β decreases with increasing fluorine concentration, while for a given F_2 concentration it increases with increasing e-beam current density. We believe that this peculiar behavior is the result of the dependence of the secondary electron energy distribution on the fluorine concentration, as will be discussed and analyzed in detail in Sec. IV.

IV. THEORETICAL ANALYSIS AND DISCUSSION

Understanding the secondary-electron kinetics in e-beam-irradiated rare-gas—halogen mixtures is essential for a complete modeling of the rare-gas—halide lasers. Most of the kinetic codes used to model these lasers assume that under attachment-dominated and steady-state conditions, the electron density is inversely proportional to the concentration of the attaching molecule.[5–10] This is true both for codes used to analyze kinetic measurements[22] and for codes used to describe the laser performance.[23] This assumption can be justified only when the attachment-rate constant is independent of the concentration of the attach-

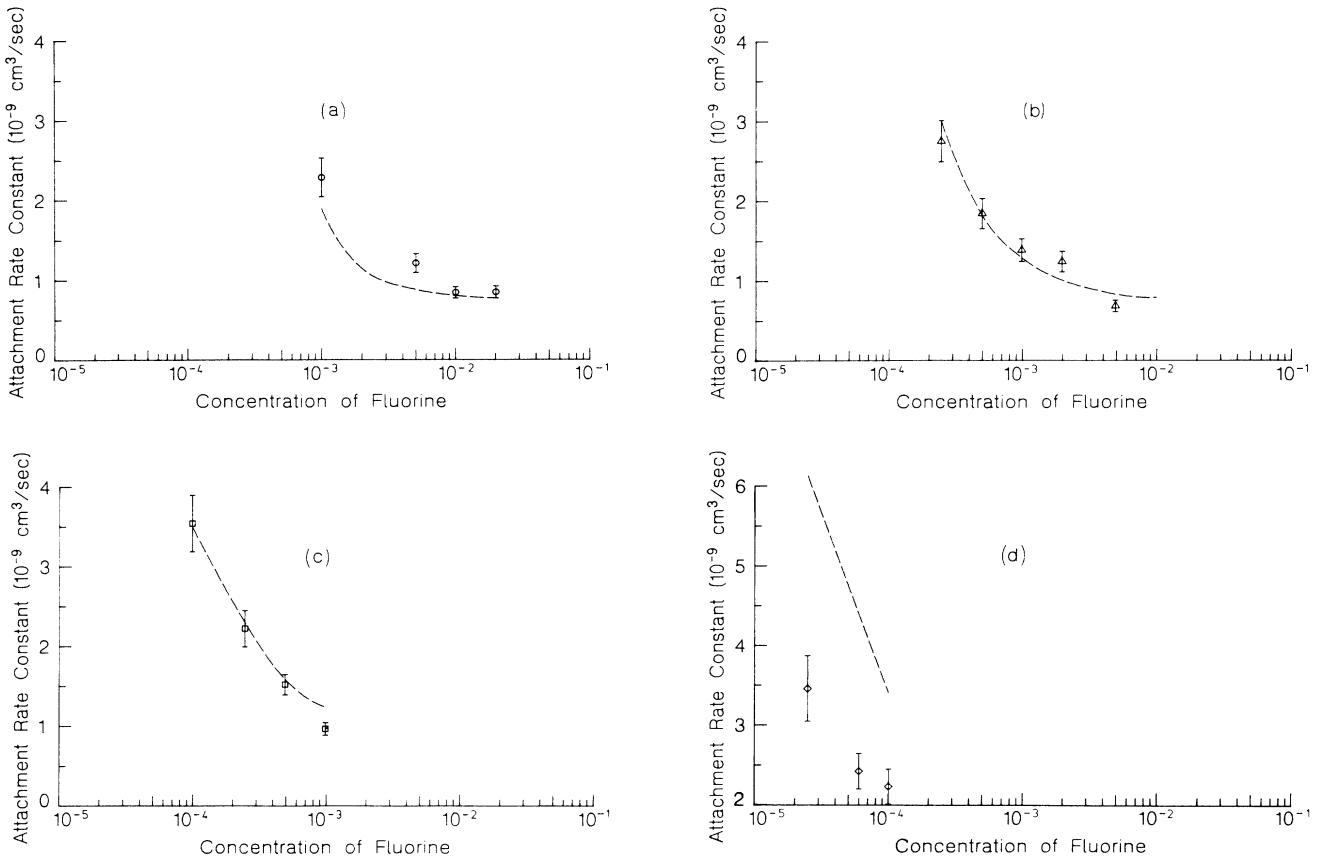

FIG. 5. Comparison of measured attachment-rate constant for fluorine, as a function of F_2 concentration with code predictions (dashed lines) for e-beam current densities of (a) 6.3 A/cm^2, (b) 0.68 A/cm^2, (c) 0.096 A/cm^2, and (d) 0.025 A/cm^2.

ing molecule. Our results show clearly a dependence of the attachment-rate constant on fluorine concentration as well as on e-beam current density. Such a dependence is expected whenever a change in the attacher concentration or in e-beam current density affects the electron energy distribution and through it the attachment-rate constant.

Before presenting a quantitative analysis of the results, it is worthwhile to discuss qualitatively some of their general features. From Fig. 5 we see that the attachment-rate constant for a given e-beam current density is a decreasing function of the fluorine concentration. On the other hand, from those portions of the figures where the fluorine concentrations overlap, we see that for a given fluorine concentration the attachment-rate constant is an increasing function of the e-beam current density. As a general trend, for average electron energies above 0.5 eV, the attachment-rate constant for fluorine is expected to decrease with increasing electron energy. This is because fluorine has a narrow cross section for dissociative attachment peaking at about 0.1 eV.[24–26] In view of that, the observed dependence of the attachment-rate constant on e-beam current density is expected because of the following reasoning. An increase in the e-beam current density increases the concentration of excited species such as Ar*, which are generated either directly by impact of fast electrons with Ar atoms[1] or by dissociative recombination of slow electrons with Ar_2^+.[19] The metastables of argon have a huge cross section of about 80 Å^2 for inelastic collision with electrons, with a threshold at 1.5 eV.[27] Thus an increase in Ar* density causes a reduction in electron average energy and a corresponding increase in the attachment-rate constant. Since the fluorine is a strong quencher of Ar*,[28] only at high current densities and with low fluorine concentrations the metastable density is large enough to affect appreciably the electron energy distribution. Because of that the dependence of the attachment-rate constant on e-beam current density is more pronounced at high e-beam currents and low fluorine concentrations as seen in Fig. 5.

The surprising aspect of the results in Fig. 5 is the fact that for a given e-beam current density, the attachment-rate constant decreases with increasing F_2 concentration. This seems to indicate that for the conditions of our experiment, the average electron energy increases with increasing fluorine concentration.

Increasing the fluorine concentration in the gas mixture affects the electron energy distribution in two ways: (a) it increases the inelastic losses such as electron-impact excitation of vibrational states of fluorine, thereby causing a reduction in the electron average energy, and (b) it increases the removal of slow electrons by attachment, thereby causing an increase in the electron average energy.

Clearly, any quantitative model for describing the results of Fig. 5 has to take into account the effect of both processes on the electron energy distribution. In the following we will compare the predictions of such a model with our experimental results.

The electron density as a function of time is given by Eq. (4). Since the attachment rate constant β and the recombination rate constant α are strongly dependent on the electron distribution function $f(\varepsilon)$, a solution of Eq. (4) necessitates the calculation of $f(\varepsilon)$ for the appropriate conditions.

When a beam of energetic electrons impinges on a gaseous target as in our experiment, the resulting processes can be divided in general into fast processes and slow processes where the characteristic time scale for the fast processes is about 2 orders of magnitude shorter then that for the slow processes. For gas mixtures containing argon with a small amount of fluorine as in our case, the fast processes include electron multiplication by ionization of ground-state argon and excitation of argon from the ground state by inelastic collisions. The energetic electrons multiply and lose energy very fast, forming an initial energy distribution function which is called the source function $f_s(\varepsilon)$.[29] The source function describes the distribution of the rate of production of the secondary electrons by the fast processes. The slow processes affecting the electron energy distribution can be divided into elastic and inelastic processes. The elastic processes include electron—heavy-particle and electron-electron collisions. The relevant inelastic processes in our case include the ionization and excitation of Ar*, vibrational and electronic excitation of fluorine, recombination of electrons with Ar_2^+, and attachment of electrons to fluorine.

The source function used for our theoretical analysis was derived by using the method described in detail by Elliott and Greene.[29] However, we made one noteworthy modification. Among the fast processes used to derive the source function, we included ionization as well as excitation of ground-state argon, while Elliot and Greene derived their source function taking into account only the ionization of ground-state argon. They included the excitation of ground-state argon among the slow processes accounted for at the second stage of the calculation of the energy distribution.[29] The reasoning behind our modification was that the cross sections for excitation and ionization of ground-state argon are of the same order of magnitude,[30] and therefore, have to be taken into account simultaneously. The source function thus obtained is plotted in Fig. 6. As expected it is truncated at 11.55 eV, which is the threshold for excitation of ground-state argon, and its average energy is 4.06 eV. Excluding the excitation of ground-state Ar resulted in a source function which was truncated at 15.75 eV (the threshold for ionization of ground-state argon), and had an average energy of 4.74 eV. We should point out that taking into account ground-state ionization and excitation consecutively rather than simultaneously one obtains a source function with an average energy of 3.8 eV. The difference between the two results is because the consecutive method does not take into account the competition between the two processes.

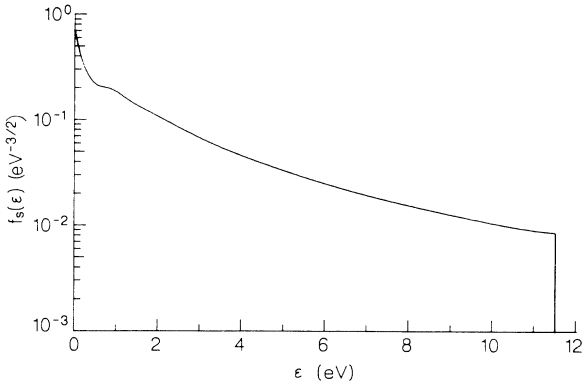

FIG. 6. Calculated source function for 1 atm of Ar irradiated by a beam of high-energy electrons.

The energy distribution function obtained as a result of the slow processes can be calculated by dividing the energy interval 0—11.55 eV into small segments with a width of $\Delta\varepsilon$, and by solving a set of rate equations for those segments. The rate equation for the electron density in the jth energy interval can be written as

$$\frac{dn_j}{dt}=R_j+S_j-W_jn_j\ , \tag{6}$$

where R_j is the rate of production of secondary electrons in the jth interval by the fast processes. S_j is the rate by which electrons are transferred to the jth interval from other intervals by elastic and inelastic collisions, and W_jn_j is the rate of removal of electrons from the jth interval by collision processes. In terms of the source function, R_j can be written as

$$R_j=R\varepsilon_j^{1/2}f_s(\varepsilon_j)\Delta\varepsilon\ , \tag{7}$$

where R is the total rate of production of secondary electrons and ε_j is the energy at the jth interval. The value used for R in our calculations was obtained from experimental measurements as described in Sec. III. Writing the right-hand side of Eq. (6) more explicitly we get

$$\frac{dn_j}{dt}=R_j+\sum_\zeta \sigma_{\zeta k}v_kn_kN_\zeta-\sum_\eta \sigma_{\eta j}v_jn_jN_\eta+(\partial n_j/\partial t)_{\rm el}$$
$$+(\partial n_j/\partial t)_{e\text{-}e}+(\partial n_j/\partial t)_{\rm SE}\ . \tag{8}$$

The second and third terms in Eq. (8) describe the effect of inelastic collisions. The fourth term is the contribution of electron—heavy-particle elastic collisions and the fourth and fifth term account for electron-electron and super elastic collisions, respectively. The second term in Eq. (8) describes the transfer of electrons to the jth interval from higher-energy intervals by inelastic collisions. $\sigma_{\zeta k}$ is the value of the cross section for the ζth inelastic process at ε_k, N_ζ is the density of the heavy particles taking part in that process, v_k and n_k are the velocity and density at the kth interval, k is determined by

$$(k-j)\Delta\varepsilon=\varepsilon_\zeta\ , \tag{9}$$

where ε_ζ is the energy loss due to the ζth inelastic processes.

Similarly, the third term in Eq. (8) describes the removal of electrons from the jth interval by inelastic processes including recombination with Ar_2^+ and attachment to fluorine. $\sigma_{\eta j}$ is the value of the cross section for the ηth inelastic process at ε_j, $N\eta$ is the density of the heavy particles taking part in that process.

The average energy-loss rate of electrons at energy ε by elastic collisions with heavy particles with mass M and density N can be written as[31]

$$\frac{d\varepsilon}{dt}=\frac{2m_e}{M}\sigma_m v\varepsilon N \ , \tag{10}$$

where σ_m is the cross section for momentum transfer. Accounting for the number of collisions necessary to lose an energy of $\Delta\varepsilon$ which is our energy resolution, the fourth term in Eq. (8) can be written as

$$(\partial n_j/\partial t)_{\rm el}=\frac{2m_e N}{M\Delta\varepsilon}[\sigma_{mj+1}v_{j+1}n_{j+1}(\varepsilon+\Delta\varepsilon) -\sigma_{mj}v_j n_j\varepsilon(1-\delta_{j,1})] \ ; \tag{11}$$

the Kronecker δ in Eq. (11) was introduced to ensure conservation of particles, while taking into account the loss of electrons by recombination and attachment. Since, as will be discussed in the following, kinetic code calculations showed that the number density of Ar*, corresponding to our experimental conditions, was below 10^{14} cm^{-3}, the super elastic term in Eq. (8) was neglected.

For electron densities of the order of magnitude 10^{14} cm^{-3} and below as in our experiments, the electron-electron collision term can be treated as a perturbation. Without the electron-electron collision term and the super elastic term, the set of Eq. (8) are linear equations that can easily be solved numerically. Taking into account the electron-electron collision term as a perturbation, using Eq. (6), the electron density at the jth interval at time $(t+\Delta t)$ can be written as

$$n_j(t+\Delta t)=\frac{R_j+S_j}{W_j}+\left[n_j(t)-\frac{R_j+S_j}{W_j}\right]e^{-W_j\Delta t} +(\partial n_j/\partial t)_{e\text{-}e}\,|_t\Delta t \ . \tag{12}$$

Equation (12) was used to incorporate the effect of electron-electron collisions on the distribution function. The method for calculation of the electron-electron collision term in Eq. (12) has been described in detail by Rockwood[32] and by Elliot and Greene[29] and will not be repeated here.

Available cross sections in the literature were used in our calculations. The momentum-transfer cross section for Ar was taken from Frost and Phelps.[33] The cross sections used for excitation and ionization of Ar* were those calculated by Hyman.[27,34] The cross section used for recombination of electrons with Ar_2^+ was derived by Bretagne *et al.*[35] Their cross section is compatible with the recombination rate coefficients given by Biondi.[19] A summary of the relevant cross sections for fluorine including momentum transfer, vibrational excitation, electron attachment, and electronic excitation to the $a\,^3\pi_u$ and $a\,^1\pi_u$ levels have been given by Hayashi and Nimura.[26] These cross sections were used in our analysis.

The densities of Ar* and Ar_2^+ were calculated by a separate kinetic code for the heavy particles. A summary of the dominant kinetic processes in an e-beam-irradiated Ar-F_2 gas mixture and their rate coefficient is given by Rokni *et al.*[36] and by Brau.[1] Because of the interdependence between the heavy-particle kinetic code and the code for calculation of the electron energy distribution, the two codes were run in a cyclic order as a function of time until convergence and steady state was attained. *A posteriori* it was found that for our experimental conditions the effect of Ar* on the electron energy distribution was important only at the highest e-beam current density used (see Fig. 3). Also, it was found that for all our experiments the contribution of recombination with Ar_2^+ to the reduction of the electron density was less then 10% of that due to attachment, as stated in Sec. III.

The code calculations showed that steady state was obtained within 20 nsec for the highest e-beam current density and within 150 nsec for the lowest e-beam current density used in our experiments. Figure 7 shows the calculated electron energy distribution function under steady-state conditions for gas mixtures containing one atmosphere Ar with 0.1% F_2 and 2% F_2 and for an e-beam current density of 6.3 A/cm^2. The comparison shows clearly the dent caused at the low-energy portion of the distribution function by the increase in the fluorine concentration. As a result the calculated average electron energy is increased from 1.97 eV for 0.1% fluorine to 2.43 eV for 2% fluorine.

The calculated values of the electron density for our experimental conditions are plotted in Fig. 3 for comparison with our experimental results. Figure 5 shows the comparison between the calculated values of the attachment coefficient to fluorine with those obtained from the experimental measurement. The theoretical values for β were

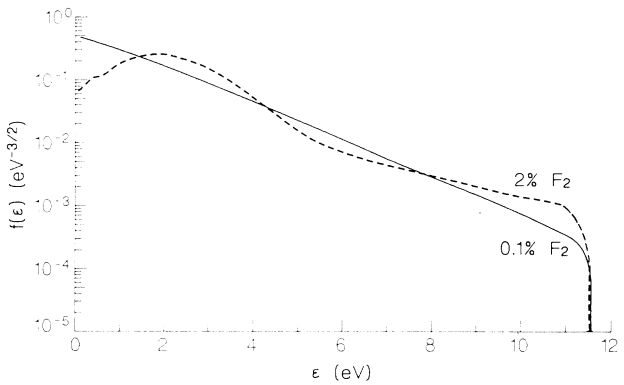

FIG. 7. Comparison between the calculated electron energy distribution functions of e-beam irradiated Ar-F_2 gas mixtures containing 0.1% F_2 and 2% F_2, for e-beam current density of 6.3 A/cm^2 and a pressure of 1 atm.

calculated from the distribution function using the expression

$$\beta = \int \sigma_a v \varepsilon^{1/2} f(\varepsilon) d\varepsilon \ , \tag{13}$$

where σ_a is the attachment cross section for fluorine.

As is seen from Figs. 3 and 5, the fit of the calculation predictions to the experimental results is very good except for the results at the lowest e-beam current density. It should be emphasized that without taking into account the effect of removal of slow electrons by attachment on the energy distribution, it was impossible to obtain a good fit of the theoretical predictions with the experimental results. The effect of increasing average electron energy with the addition of a strong electron attacher to a gas mixture has been proposed in the past in a model for e-beam-irradiated rare gas and NF_3 mixtures.[37] But to our best knowledge our results are the first experimental manifestation of this effect.

V. CONCLUSION

We have measured the electron density in electron-beam-irradiated Ar-F_2 gas mixtures for the first time, using time-resolved infrared interferometry. From the dependence of the measured steady-state electron density on the fluorine concentration, we have determined the attachment-rate constant for fluorine at zero electric field for the first time. The results show a dramatic dependence of the attachment-rate constant on fluorine concentration and on the e-beam current density. Using a kinetic code for calculation of the electron energy distribution, we have shown that this dependence is a manifestation of the variation of the electron energy distribution as a function of e-beam current density and fluorine concentration. From our model calculations we conclude that the net effect of increasing fluorine concentration at low concentrations is an increase in the electron mean energy caused by fast removal of low-energy electrons. This effect and the dependence of the attachment-rate constant on the fluorine concentration must be incorporated in codes used to model laser performance as well as in codes used to analyze kinetic processes involving secondary electrons. For example, Trainor *et al.*[4] measured the quenching rate of ArF* and KrF* by secondary electrons. For the derivation of rate constants they calculated the electron density assuming it was inversely proportional to the attacher concentration. Taking into account the variation of the attachment-rate constant with fluorine concentration would reduce their rate constants for quenching of ArF* and KrF* by electrons by almost a factor of 2.

ACKNOWLEDGMENTS

We wish to thank Dr. J. H. Jacob for informative discussions and Mr. J. Rosenfeld for technical assistance. One of the authors (M. Rokni) also thanks Dr. D. Reilly for discussions on the time-resolved interferometry technique. This work was supported by the U.S.—Israel Binational Science Foundation (BSF), Jerusalem.

[1]See, for example, the following reviews and the references therein: (a) C. H. Brau, in *Excimer Laser*, edited by Ch. K. Rhodes (Springer-Verlag, New York, 1979), Chap. 4; (b) M. Rokni and J. H. Jacob, in *Applied Atomic Collision Physics*, edited by H. S. W. Massey, E. W. McDaniel, and B. Bederson (Academic, New York, 1982), Vol. III, Chap. 10.

[2]A. V. Hazi, T. N. Rescigno, and A. E. Orel, Appl. Phys. Lett. **35**, 477 (1979).

[3]D. W. Trainor, J. H. Jacob, and M. Rokni, J. Chem. Phys. **72**, 3646 (1980).

[4]D. W. Trainor and J. H. Jacob, Appl. Phys. Lett. **37**, 675 (1980).

[5]J. H. Jacob and J. A. Mangano, Appl. Phys. Lett. **28**, 724 (1976).

[6]W. H. Long, Jr., Appl. Phys. Lett. **31**, 391 (1977).

[7]M. Rokni, J. A. Mangano, J. H. Jacob, and J. C. Hsia, IEEE J. Quantum Electron. **QE-14**, 464 (1978).

[8]W. L. Nighan, IEEE J. Quantum Electron. **QE-14**, 714 (1978).

[9]D. E. Klimek, J. C. Hsia, J. H. Jacob, D. W. Trainor, C. Duzy, and H. A. Hyman, IEEE J. Quantum Electron. **QE-17**, 1847 (1981).

[10]F. Kannari, A. Suda, S. Yamaguchi, M. Obara, and T. Fujioka, IEEE J. Quantum Electron, **QE-19**, 232 (1983).

[11]See, for example, S. C. Brown, *Introduction to Electrical Discharges in Gases* (Wiley, New York, 1965).

[12]H. L. Chen, R. E. Center, D. W. Trainor, and W. I. Fyfe, Appl. Phys. Lett. **30**, 99 (1977).

[13]D. W. Trainor and J. H. Jacob, Appl. Phys. Lett. **35**, 920 (1979).

[14]K. J. Nygaard, S. R. Hunter, J. Fletcher, and S. R. Foltyn, Appl. Phys. Lett. **32**, 351 (1978); see also, K. J. Nygaard, H. L. Brooks, and S. R. Hunter, IEEE J. Quantum Electron. **QE-15**, 1216 (1979).

[15]B. I. Schneider and C. A. Brau, Appl. Phys. Lett. **33**, 569 (1978).

[16]By the term specific refractive index of an excited state we mean the contribution of one excited atom in this state to the refractive index.

[17]W. L. Weise, M. W. Smith, and B. M. Miler, *Atomic Transition Probabilities*, Natl. Bur. Stand. (U.S.) Circ. No. 22 (U.S. GPO, Washington, D.C., 1969), Vol. II, p. 187.

[18]See, for example, M. Born and E. Wolf, *Principles of Optics*, Sixth ed. (Pergamon, New York, 1980), Chap. VII.

[19]M. A. Biondi, *Applied Atomic Collision Physics*, edited by. H. S. W. Massey, E. W. McDaniel, and B. Bederson (Academic, New York, 1982), Vol. III, Chap. 6.

[20]See, for example, J. H. Jacob, J. Appl. Phys. **45**, 467 (1974).

[21]M. Tekula (private communication).

[22]See, for example, Refs. 3, 4, and 8.

[23]See, for example, Refs. 5, 7, and 10.

[24]W. C. Tam and S. F. Wong, J. Chem. Phys. **68**, 5626 (1978).

[25]P. J. Chantry, Bull. Am. Phys. Soc. **24**, 134 (1979).

[26]M. Hayashi and T. Nimura, J. Appl. Phys. **54**, 4880 (1983).

[27]H. A. Hyman, Phys. Rev. A **18**, 441 (1978).

[28]J. E. Velazeo, J. H. Kolts, and D. W. Setser, J. Chem. Phys. **65**, 3468 (1976).

[29]C. J. Elliot and A. E. Greene, J. Appl. Phys. **47**, 2946 (1976).
[30]L. R. Peterson and J. E. Allen, Jr., J. Chem. Phys. **56**, 6068 (1972).
[31]See, for example, H. S. W. Massey and E. H. S. Burhop, *Electronic and Ionic Impact Phenomena* (Oxford University Press, London, 1969), Vol. 1, Chap. 2.
[32]S. D. Rockwood, Phys. Rev. A **8**, 2348 (1973).
[33]L. S. Frost and A. V. Phelps, Phys. Rev. **136**, A1538 (1964).
[34]H. A. Hyman, Phys. Rev. A **20**, 855 (1979).
[35]J. Bretagne, J. Godart, and V. Puech, J. Phys. D **15**, 2205 (1982).
[36]M. Rokni, and J. H. Jacob, and J. A. Mangano, Phys. Rev. A **16**, 2216 (1977).
[37]L. J. Denes, S. G. Leslie, L. E. Kline, and L. A. Weaver, *Proceedings of the International Conference on Lasers 1979,* p. 203.